Nuclear Instruments and Methods in Physics Research A 737 (2014) 195–202

Contents lists available at ScienceDirect

Nuclear Instruments and Methods in Physics Research A

journal homepage: www.elsevier.com/locate/nima

OFFSET: Optical Fiber Folded Scintillating Extended Tracker

D. Lo Presti [a,b,*], S. Aiello [b], D.L. Bonanno [a], G.A.P. Cirrone [c], E. Leonora [b], F. Longhitano [b], C. Pugliatti [a,b], N. Randazzo [b], F. Romano [c], G.V. Russo [a,b], M. Russo [a,b], C. Stancampiano [c], V. Sipala [d,e]

[a] University of Catania, Catania, Italy
[b] INFN - Sezione di Catania, Catania, Italy
[c] LNS, Catania, Italy
[d] University of Sassari, Sassari, Italy
[e] INFN - Sezione di Cagliari, Cagliari, Italy

The OFFSET Collaboration

ARTICLE INFO

Article history:
Received 6 August 2013
Received in revised form
13 November 2013
Accepted 13 November 2013
Available online 23 November 2013

Keywords:
Scintillating fiber
Tracking detector
Real-time

ABSTRACT

The OFFSET collaboration aims at the development of a novel system for tracking charged particles, designed to achieve real-time imaging, large detection areas, and a high spatial resolution especially suitable for use in medical diagnostics. This paper presents the first prototype of this tracker, having a $20 \times 20\ cm^2$ sensitive area made by two crossed ribbons of 500 μm square scintillating fibers. The track position information is extracted in real time using a reduced number of read-out channels to obtain very large detection area at moderate cost and complexity. The performance of the tracker was investigated using β sources, cosmic rays and a 62 MeV proton beam.

1. Introduction

Cutting edge research in the treatment of tumors has been oriented toward hadron therapy, one of the most effective external radiotherapy techniques, which uses charged particle beams (protons and carbon ions) with up to 400 A MeV energy [1]. Such beams make it possible to accurately release the required dose to the cancerous mass, leaving at the same time the surrounding healthy tissue almost totally untouched. The maximum advantage from the use of charged particle beams is reached when there is precise information about the stopping power of the particles used for the radiotherapy treatments. The direct use of this information, rather than that from X-ray tomography, leads to a more accurate evaluation of the distribution of the dose and can be used to verify the positioning of the patient. Therefore, the availability of very accurate particle imaging systems is of fundamental importance [2]. Our task is to design and build an imaging system for charged particles based on the consolidated principle of residual range measurement [3], taking advantage of new detection techniques. The aim is to use this system to achieve large detection areas (up to $30 \times 30\ cm^2$) suitable for almost all medical physics applications, high spatial resolution (up to 150 μm, given by dividing the employed scintillating fibers (Sci-Fi) size by $\sqrt{12}$) and excellent time resolution (up to 2 ns). With this objective in mind, we have designed and developed a prototype of an $X-Y$ tracker [4–6], the OFFSET (Optical Fiber Folded Scintillating Extended Tracker) detector, mainly funded by the Istituto Nazionale di Fisica Nucleare, which has been accurately tested with radioactive sources, cosmic rays and the 62 MeV proton beam, available at the Laboratori Nazionali del Sud (LNS) CATANA proton therapy facility.

2. OFFSET

The OFFSET detector consists of two planes of Sci-Fi orthogonal one to each other. The sensitive $20 \times 20\ cm^2$ area was built employing 500 μm square multicladding BCF-12 [7] Sci-Fi, manufactured by Saint-Gobain. In these fibers, the energy released by a crossing particle produces an isotropical emission of light. A part of this light will be channelled into the fiber, which at this point will act as a guide. This light will be transported by the mechanism of total internal reflection in both directions along the fiber.

* Corresponding author at: University of Catania, Catania, Italy.
Tel.: +39 0953785413; fax: +39 0953785240.
E-mail addresses: domelop@gmail.com, domenico.lopresti@ct.infn.it (D. Lo Presti).

0168-9002/$ - see front matter © 2013 Elsevier B.V. All rights reserved.
http://dx.doi.org/10.1016/j.nima.2013.11.049

The factory can deliver the fibers as pre-glued and aligned ribbons. In the literature, the Sci-Fi with cross-section equal or bigger than one millimeter squared has been very well characterized to extract the absorbtion length [8]. For the Sci-Fi with a lower section area we made an accurate study [9]. Many technical constraints limit the maximum reachable sensitive area. As reported in [9], the attenuation length measured for the BCF12 fibers, square cross-section and 500 μm thick, is about 1 m. Choosing a maximum length of the Sci-Fi that is equal to the attenuation length of 1 m, one can evaluate the maximal possible dimensions of the sensitive area, taking also into account the length of scintillating fiber needed for routing to the optical sensor. This last length can be estimated by fixing the bending radius and considering the path from the last fiber of the ribbon to the opposite edge of the sensitive area (see Fig. 1). The maximum possible size for the sensitive area, calculated in this way, is about 45×45 cm^2. The dimensions of the OFFSET tracker are well below these limits.

We have arranged two 400 fiber ribbons in orthogonal layers, one above the other, kept in position by the pressure of two square aluminum frames, delimiting the sensitive area of the detector. Fig. 1 shows two pictures of the final detector. In (a), without cover, the sensitive 20×20 cm^2 area, made of Sci-Fi, is visible. The routed clear fibers outside the sensitive area are also visible. In (b) an outside view of the detector with the front-end board is shown. The total size of the detector, including the mechanical structure, is 70×100 cm^2.

In a classical read-out scenario, every Sci-Fi must be optically coupled to a light sensor and the signal recorded by a single channel of the front-end electronics. In the case of the 20×20 cm^2 prototype there are 800+800 channels, considering the coincidence between the signals coming from both edges of each Sci-Fi. A suitable read-out system would not only be complex but also expensive. Instead, we use a readout solution that is a good compromise between cost and dead time.

2.1. Channel reduction system

The OFFSET tracker uses a read-out channel reduction architecture that is suitable for imaging conditions. This architecture reduces the number of read-out channels for a linearly segmented detector and is a modern version of previous applications [10,11]. The operating principle of the channel reduction is explained below. Let us consider a strip detector. It detects one particle at a time. Each strip is read from both ends and the signals are grouped in a special way, which results in a significant lower number of readout channels compared to those when each strip is readout at one end with a dedicated readout channel. All strips on one end are read out in groups of n neighboring strips, named *NeigSet*, while at the other end the first strips of each group are grouped in *StripSet*1, the second strips of each group in *StripSet*2, and so on to n (see Fig. 2). This implies that the number of readout channels on the second side is equal to the number of fibers per channel on the first side. A particle crossing one strip generates a signal at both ends of the fiber. Then we have a signal from the ıth *NeigSet* group and another from the jth *StripSet* that univocally identifies the Strip_{hit} hit, according to the following equation:

$$\mathbf{Strip_{hit}} = (i-1) \times n + j \tag{1}$$

An $X-Y$ strip detector with 16 strips for each plane is shown in Fig. 2, as an example of a two-dimensional strip detector where the channel reduction system is applied. In a classical read-out scheme of a two-dimensional strip detector with 16 strips in each dimension, there would be 16 read-out channels for the X direction and 16 for the Y direction, making a total of 32 channels. The proposed readout scheme reduces the number of readout channels to 16. In general the number of readout channels needed to read out both dimensions with this scheme is $4\sqrt{N}$, where N is the total number of strips per layer, X or Y. When N is large the reduction factor becomes important, in light of the goal of real time acquisition. An additional advantage of this readout scheme is that the required readout of the signal at both ends of a fiber significantly reduces accidental triggers due to noise, crosstalk, dark counts, etc. Notice that to reconstruct the point where the particle crosses the detector (event), we need an energy release in both planes.

The application of a read-out channel reduction consists in suitably grouping and coupling the Sci-Fi to larger section standard (clear) optical fibers. Each group of n Sci-Fi is coupled to an ESKA CK-100 clear fiber [12] that is coupled to a light sensor. Fig. 3 shows the scheme of the optical coupling (a) and a picture of one Sci-Fi bundle machined and ready for coupling (b). In the OFFSET tracker the application of the read-out channel reduction system could result in a minimum of 80 readout channels. However, in order to fit the clear fiber to the pixel size of the used photomultiplier and maximize the acquisition rate, the detector was segmented in 16 independent sub-detectors. The segmentation and the application of the channel reduction scheme result in a total of 160 read-out channels, which is exactly one-fifth of the channels that would be needed if no channel reduction scheme

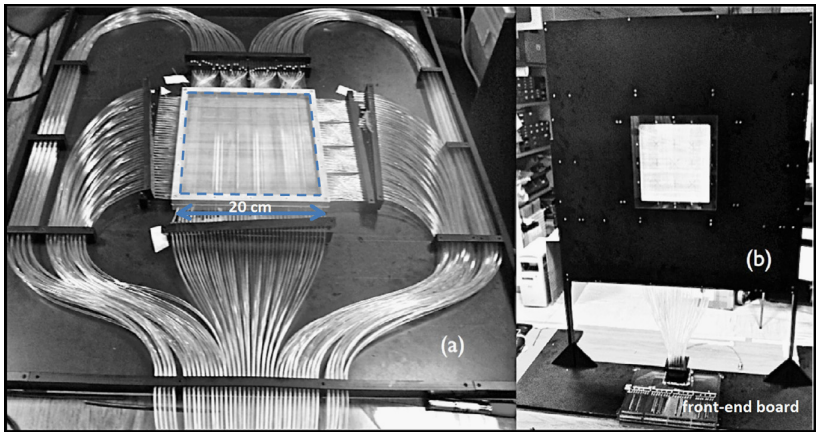

Fig. 1. (a) The OFFSET tracker without the cover. The dashed sensitive 20×20 cm^2 area, made of Sci-Fi, is visible. The clear fibers routing is also shown. (b) The fully assembled OFFSET tracker.

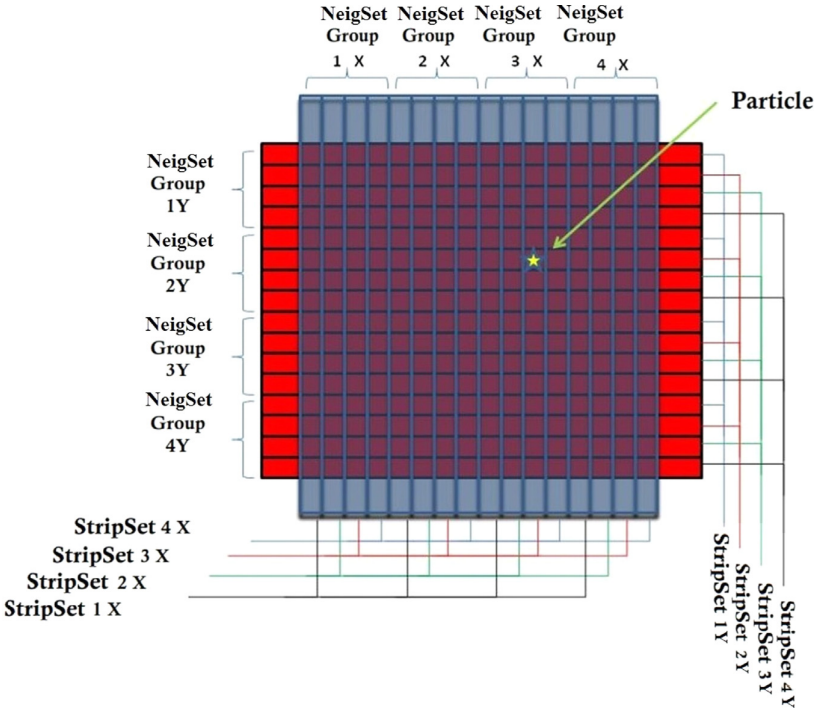

Fig. 2. An example of the application of the channel reduction scheme.

would be applied. Indeed, dividing the 1600 channels in 16 sub-groups and applying the reduction system explained in Eq. (1), then we have 10 channels for each layer sub-group and so 160 read-out channels.

2.2. Photosensor

A single multianode photomultiplier (PSPM) is used as a light sensor. We have chosen the 16×16 pixels H9500 PSPM Hamamatsu photomultiplier [13]. It needs only one high voltage power supply, provides a signal for each pixel, and one additional signal, called the dynode, which is the analog sum of the signals of the last dynode of all the PSPM channels. In the OFFSET detector, 10 Sci-Fi are coupled to one single clear fiber that is about 1 m long. The light from the scintillating fibers propagates 1 m through the clear fibers to one pixel of the PSPM. The coupling is made by mechanically routing and fixing the Sci-Fi and clear fibers and applying optical gel between them. The maximum possible cross-section of a clear fiber and, therefore, the number of Sci-Fi coupled to one clear fiber is determined by the pixel size of the selected photomultiplier, which is about 2.8×2.8 mm^2.

2.3. Front-end electronics

The detector signals are processed with a simple digital acquisition. The PSPM is housed into a front-end board. Each anode signal is connected to one of the four inputs of a MAX964 comparator [14] shunted by a suitable resistor. We have chosen the value of this resistance for all channels as a compromise between the amplitude and the timing characteristics of the anodic voltage signal [15]. The optimal value of the shunt resistor is 200 Ω. This leads to a single photoelectron signal with about 5 mV amplitude (with a PSPM gain of about 2×10^6) and about 8 ns Full Width Half Maximum (FWHM). The output of each comparator is then sent to a monostable, which stretches the comparator output signal to 100 ns. The stretched comparator signal affects the detector efficiency at event rates higher than 10 MHz. All the 160 outputs of the front-end board are then transmitted through shielded cables to the data acquisition board. A common comparators threshold is set to about 1/3 of the single photo-electron mean peak amplitude.

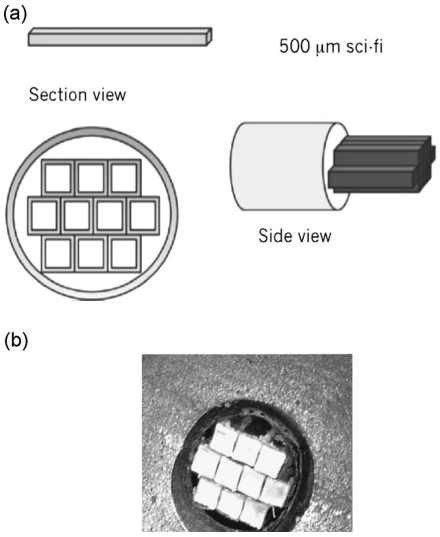

Fig. 3. (a) The scheme of the optical coupling between the 10 Sci-Fi and the optical fiber. (b) A picture of one Sci-Fi bundle after it has been machined for coupling.

2.4. Data acquisition

The comparator signals are processed with a simple digital electronics to perform pre-analysis, filtering, and storage on a PC. The comparator signals from the front-end board are fed into a data acquisition module, a real-time FPGA PXI-7813R [16]. This module

has 160 digital inputs/outputs, that can be sampled up to 40 MHz and supports real-time analysis and Direct Memory Access (DMA) transfer to mass storage. The real-time analysis allows us to distinguish between single and multi-hits and decode the x–y position. In our setup we use a sampling frequency of 25 MHz which is the reason why we stretched the comparator outputs to 100 ns. With a sampling frequency of 25 MHz we are able to distinguish two events whose time of arrival difference is more than 40 ns. The contribution to the jitter of the arrival time due to the PSPM, fibers and noise is negligible (<1 ns). One main requirement for our application is to achieve an acquisition rate of 1 million of events per second [2] so a tradeoff between the average particles rate and the acquisition rate must be found. From our calculations, taking into account the Poisson distribution of the time of arrival of the particle, at 1 MHz rate (average) the acquisition efficiency is about 90%. However the data acquisition board, PXI-7813, has a limitation in the data transfer bandwidth and this is why we worked at 300 kHz average event rate. Using a better performing data acquisition module and eliminating the 100 ns signal stretching, it would be possible to increase the acquisition rate up to 100 MHz, which is the rate when a significant overlap between the PSPM signals of different events would occur. A real time module, a PXIe-8102, is interfaced to the PXI-7813R through the PXI bus. The PXIe-8102 manages the DMA and the PXI bus, the ethernet communication for the remote host control and data processing thanks to its real-time operating system. Finally, it stores data to a solid state hard disk. The PXI-7813R continuously monitors the 160 digital input lines. The identification of a pattern of at least 4 coincident high logic signals, determines the trigger condition of the system. We have developed the firmware and the software for the OFFSET tracker data acquisition, analysis, display and control, using the LabView software platform.

3. OFFSET Tests

Simulation studies with the GEANT4 toolkit [17] of the OFFSET tracker do not allow us to draw quantitative conclusions on the detector response and performances. However, the scientific literature [8,18] provides some essential reference points needed for the design of the detector. With the aim of choosing the optimal design of the detector and to characterize it, the OFFSET tracker was intensively tested using β sources, cosmic rays, and a 62 MeV proton beam.

3.1. Tests using sources and cosmic rays

At first we have tested the OFFSET detector using β sources and cosmic rays. The use of β sources is very useful because it allows an image to be produced in the worst possible conditions, i.e. with particles that produce a low level of scintillation light.

Fig. 4 shows an image of a ^{90}Sr β source with an activity of 3 kBq and a diameter of 2 cm, placed closely in front of the sensitive area of the detector. The missing lines correspond to a bad optical contact of one of the forty *StripSet* somewhere between the Sci-Fi bundle and the PSPM. This is due to the Sci-Fi routing procedure. This test shows that the detector is sensitive to beta particles and then, therefore, can be used for the characterization of OFFSET if no proton beam is available. An important test is the response of the detector to cosmic rays, because these are minimum ionizing particles (MIP) with low energy deposit inside the fibers and an exposure of OFFSET that is uniform over the entire sensitive area of the detector. Notice that, a 250 MeV proton beam for medical imaging deposits an energy equivalent of 2 MIP in OFFSET. In Fig. 5, the x and y projections of the cosmic rays image, acquired in 47 h, are shown. The histograms provide information about the uniformity in the detector response. Four groups of

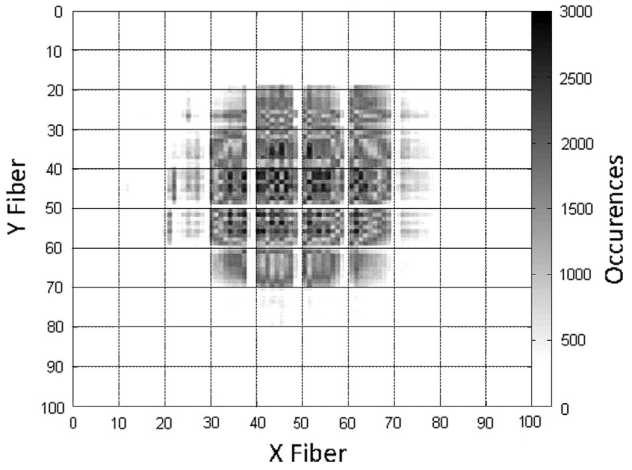

Fig. 4. A 2D real time image of a ^{90}Sr beta source acquired with the OFFSET tracker. Axis unit is in fibers number. The size of one fiber is 500 μm. The source activity is 3 kBq and the exposure time, needed to reach the three million of events prefixed for the image, is of about 30 min.

Sci-Fi, ten Sci-Fi each, are absent in the image. This is due to the failure of the corresponding front-end channels. Some lines in the x and y direction are also missing for the same reason as in the case of the test with beta sources. The average value of hits on single fiber is 1645 with a standard deviation equal to 448 (27.2%) for x projection and 1609 and 435 (27%) for y projection. The non-uniformity in the detector response is mainly due to the different optical coupling between the fibers and the PSPM and to the different gain factor of the PSPM channels.

3.2. Test with 62 MeV protons

The prototype of the detector has also been tested with a 62 MeV proton beam in the CATANA facility, at the LNS in Catania [19]. Just before starting the measurement with the OFFSET tracker, during the same run of measurements, the CATANA staff performed a beam profile characterization along the x and y directions, with calibrated diodes. The result is shown in Fig. 6. A long run of about 60 min, with a total dose accumulated of about 1.2 Gy, was performed using a 1.5 cm diameter hole calibrated collimator. During this run an image of the beam after the collimator was recorded with the OFFSET detector in real time every minute, integrating the occurrences of reconstructed tracks over the time interval. Setting the beam intensity to achieve an event rate of about 300 kHz, the time needed to acquire an image with sufficient statistics, about 1 million of events, is about 3 s. In order to perform a precise calibration of the detector, a gafchromic EBT3 film [20] was placed in front of the sensitive area crossed by the proton beam. Fig. 7 shows a sketch and the picture of the experimental setup. The calibrated gafchromic EBT3 film was digitized with a scanner and the final dose distribution was used to calibrate the region of the sensitive area of the OFFSET tracker that intersected with the beam. For the calibration of the images acquired by the OFFSET detector two assumptions have been done: a linear response of the scintillating fiber with respect to the received dose in the selected dose range and the same efficiency of each detector pixel. The calibration was performed by summing, pixel by pixel, all the images acquired with OFFSET, based on the reasonable assumption that any non-uniformity in the pixel response in the sensitive area was time invariant. In this way a calibration matrix is obtained that provides relative correction factors for each pixel of the OFFSET tracker.

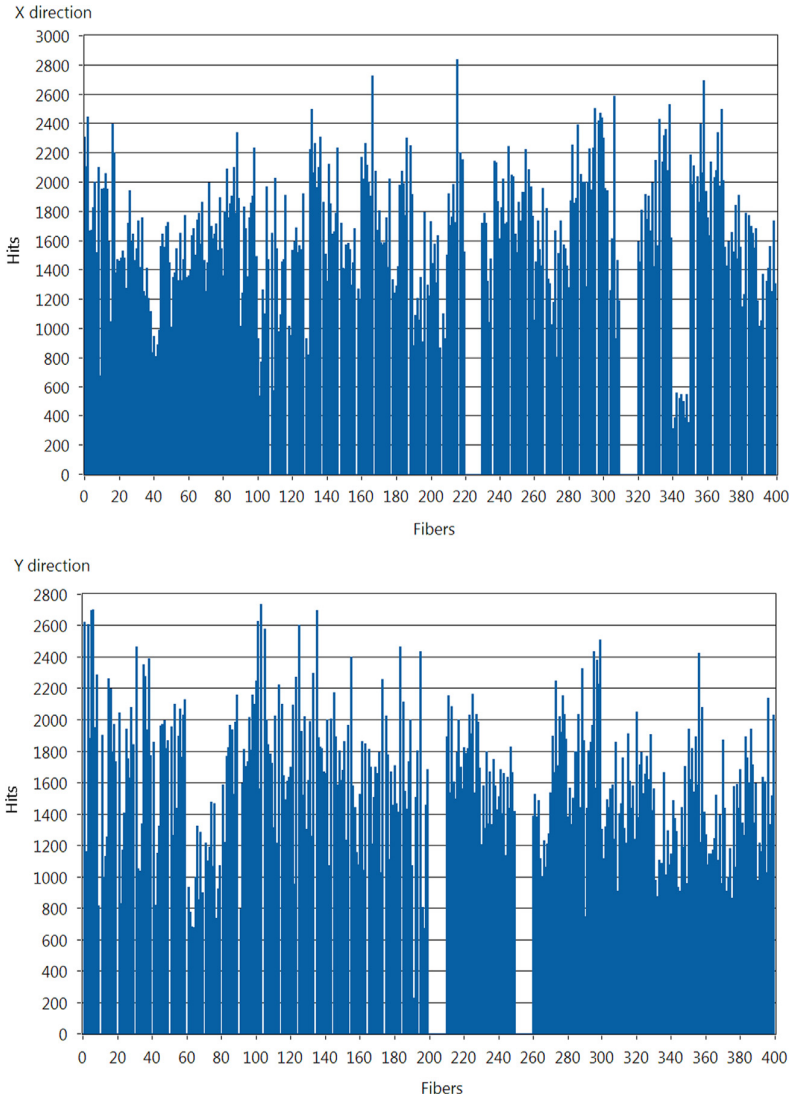

Fig. 5. Histograms for the *x* and *y* directions of the image of cosmic rays acquired by the OFFSET tracker.

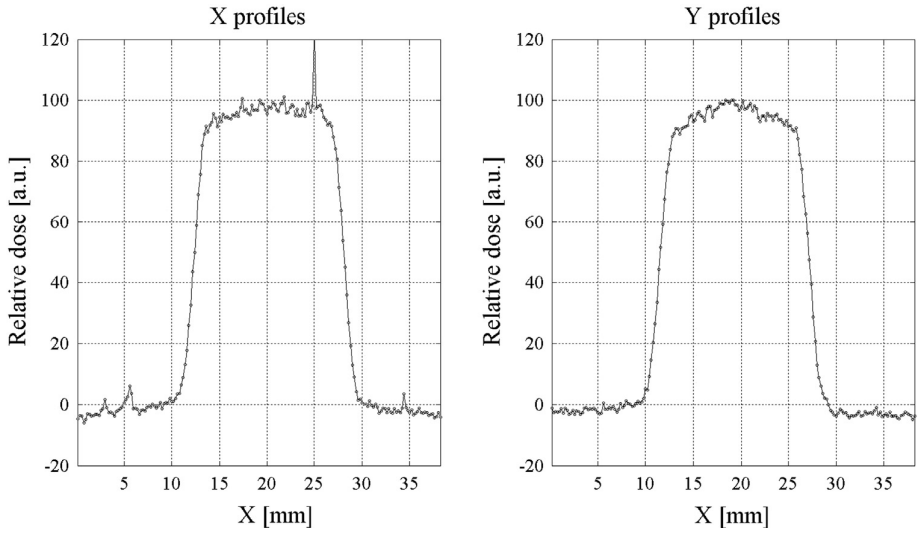

Fig. 6. Beam profile characterization acquired with calibrated diodes.

The calibration matrix is used to correct non-uniformities in the detector response due, as already mentioned in the previous section, to inhomogeneities in the optical coupling between the fibers and the PSPM and non-uniformity of the PSPM gain. Unlike in the measurements with cosmic rays, in this case no missing fiber groups were present, thanks to the repair of the front-end board. The preliminary results of the beam test of the detector, with the front-end board repaired, are presented in Fig. 8. The improvement in uniformity with respect to the uniformity obtained with cosmic rays and the beta source is clearly visible. The two profiles of the beam after the collimator, in the x and y direction, are extracted from the OFFSET calibrated frames and the gafchromic image. The profiles are normalized to the center axis and interpolated with a linear function. Penumbra and field size are calculated on the profiles. The penumbra is defined as the distance in mm between the points corresponding to 20% and 80% of the dose value on the central axis, while the size of the field is defined as the distance in mm between the points corresponding to 50% of the dose values. In Table 1, the measured left and right penumbra and the field size are reported. Further analysis is in progress to characterize uniformity and symmetry of the image. After calibration, each 1-min frame recorded with OFFSET was analyzed in order to perform a beam profile characterization as a function of time. Fig. 9 shows the x and y beam profile of a frame. In the analysis the missing lines whose corresponding values are equal to zero have been removed.

To evaluate the effectiveness of the calibration, another long run, of about 1.6 Gy, has been taken, using an eye-shaped collimator (that was used during a proton therapy treatment, according to a tumor shape). The same calibration matrix obtained in the previous measurement in the proton beam was used to correct the image of the eye-shaped collimator and the results are shown in Fig. 10. By comparing the beam profile measured with the film with the one acquired with OFFSET we extract the imaging performance of the tracker.

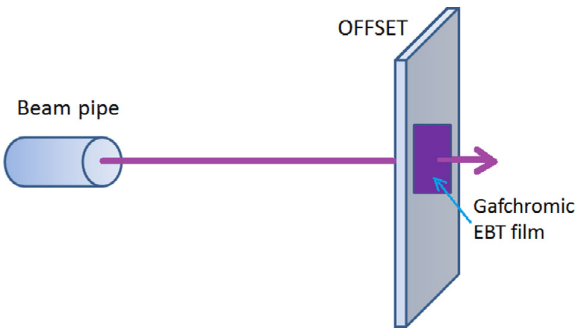

Fig. 7. Drawing of the experimental setup inside the CATANA hadron therapy facility.

3.3. Efficiency

In order to determine the detection efficiency of the prototype, we measured the rate of the particles that crossed the sensitive area of the detector by a Constant Fraction Discriminator (r_{CFD}) setting a threshold of about 1/3 of the single photo-electron. The measured rate is due to the light produced in the scintillating fibers. The measurement was performed using the dynode signal of the PSPM connected to the input of a SensL CFD [21]. The r_{CFD} was compared to the rate measured with a plastic scintillator read by a bialkali photomultiplier, that was placed after the OFFSET tracker downstream of the beam. Correcting for the dead area of the detector (mainly due to the cladding), the two measured rates were about the same (the ratio of the rates is about 0.9 and the dead area due to the cladding about 10%). Therefore r_{CFD} was taken as the reference value for the detector efficiency calculation.

Then we measured the rate r_{Tr} of tracks recorded by the detector read-out using the trigger condition described in Section 2.4. As can be seen in Fig. 8a, some events are missing due to the lack of some vertical and horizontal lines. We have estimated the rate r_{Te} of tracks in these lines to be the average of the neighbor pixels. In this way, the total rate r_{Tt} of tracks can be evaluated as the sum $r_{Tr} + r_{Te}$. Then the detection efficiency of the sensitive area η_D is expressed by the ratio r_{Tt}/r_{CFD}, which results to be 80.5%. As already mentioned the sensitive area of the detector is reduced by the multicladding of the fiber, which is naturally not taken into account by r_{CFD}. In an $X-Y$ square detector with length L that utilizes square fibers of thickness t_f with a multicladding that is t_c thick, the active area can be calculated as

$$S_A = \left(1 - 2\frac{t_c}{t_f}\right)^2 L^2. \quad (2)$$

Table 1
Profile characterization results.

Parameter [mm]	GAF	OFFSET
X projection		
Left penumbra	2.4	2.6
Right penumbra	2.2	3.6
Field width	20.9	20.6
Y projection		
Left penumbra	2.3	3
Right penumbra	2.15	3
Field width	21	21

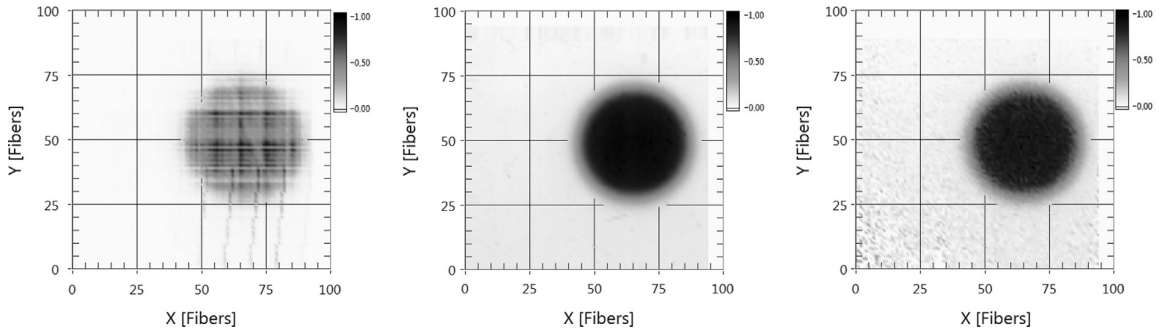

Fig. 8. Images obtained with a 62 MeV proton beam: (left) the raw sum of all the images recorded with OFFSET; (center) the gafchromic EBT3 film image; (right) the sum of all the frames acquired by OFFSET, after calibration. Axes are in fiber number (one fiber has a diameter of 500 μm).

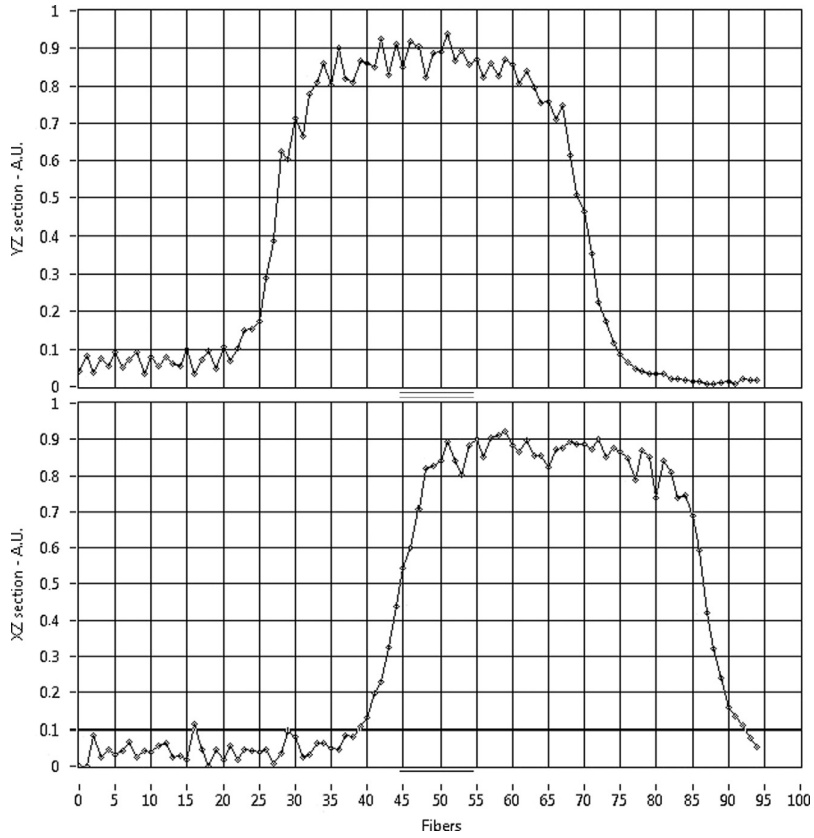

Fig. 9. x and y beam profile of a frame acquired by OFFSET tracker. The profile was monitored during time by the detector.

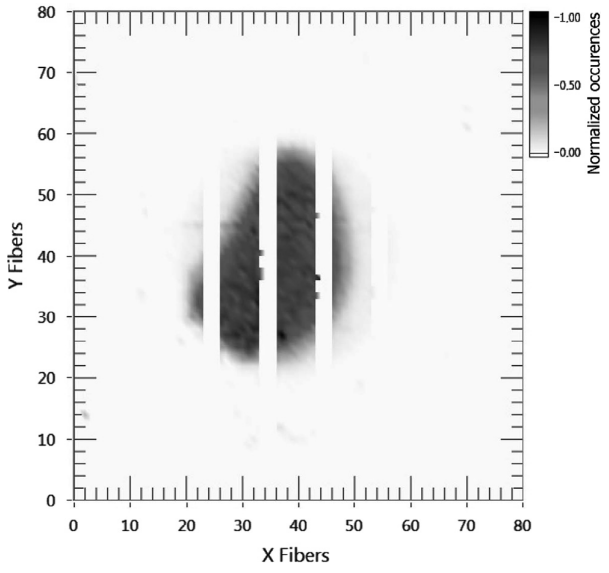

Fig. 10. The eye-shaped collimator image, calibrated. Axes are in fiber number (each fiber has a diameter of 500 μm).

From which the geometric efficiency η_G follows as

$$\eta_G = \left(1 - 2\frac{t_c}{t_f}\right)^2. \quad (3)$$

In our fibers $t_c/t_f = 0.06$ and then η_G can be evaluated as about 77%. Accordingly, the total detection efficiency η_T of the OFFSET tracker is

$$\eta_T = \eta_D \times \eta_G. \quad (4)$$

Notice that the η_G is lower than the ratio between r_{CFD} and the rate measured with the plastic scintillator because not all the events counted by the CFD can be reconstructed, as explained in Section 2.1, by the decoding algorithm.

With all the channels operational, we would expect 0.8×0.77 equal to 62% efficiency.

4. Conclusion and outlook

The first prototype of the OFFSET tracker was designed and tested with beta sources, cosmic rays, and proton beams. It has the great advantage of a read-out channel reduction system applied to a large area detector with a high spatial resolution, employing submillimeter Sci-Fi. A complete characterization was carried out and the results were presented. In order to reduce its overall size and to improve its imaging performance with a large sensitive area (30×30 cm^2) a new version of the detector is now under construction. The obtained results demonstrate the validity of the designed read-out technique, which has been patented by the Istituto Nazionale di Fisica Nucleare (INFN) [22].

Acknowledgments

The OFFSET project is a 3 years project funded by INFN National Scientific Committee V (technological and inter-disciplinary research).

References

[1] R. Pleskac, et al., Nuclear Instruments and Methods in Physics Research Section A 678 (2012) 130, http://dx.doi.org/10.1016/j.nima.2012.02.020.
[2] G.A.P. Cirrone, et al., Nuclear Instruments and Methods in Physics Research Section A: Accelerators, Spectrometers, Detectors Associated Equipment 576 (2007) 194, http://dx.doi.org/10.1016/j.nima.2007.01.151.
[3] D.A. Watts, U. Amaldi, et al., A proton range telescope for quality assurance in hadrontherapy. TERA Found., Chile: Nuclear Science Symposium Conference Record (NSS/MIC), Oct. 24 2009–Nov. 1 2009, pp. 4163–4166, http://dx.doi.org/10.1109/NSSMIC.2009.5402303.
[4] B. Beischer, et al., Nuclear Instruments and Methods in Physics Research Section A: Accelerators, Spectrometers, Detectors Associated Equipment 622 (3) (2010) 542, http://dx.doi.org/10.1016/j.nima.2010.07.059.
[5] K2K Collaboration, Nuclear Instruments and Methods in Physics Research Section A: Accelerators, Spectrometers, Detectors Associated Equipment 453 (2000) 165, http://dx.doi.org/10.1016/j.brr.2011.03.031.
[6] R.C. Ruchti, Annual Review of Nuclear and Particle Science 46 (1996) 281.
[7] Saint Gobain Crystals – Scintillating optical fibers brochure: ⟨http://www.detectors.saint-gobain.com⟩.
[8] Z. Papandreou, et al., Nuclear Instruments and Methods in Physics Research A 596 (2008) 338.
[9] D. Lo Presti, et al., Characterization technique of sub-millimeter scintillating fibers, IEEE Nuclear Science Symposium/Medical Imaging Conference (NSS/MIC)/18th International Workshop on Room-Temperature Semiconductor X-Ray and Gamma-Ray Detectors, Valencia, Spain, Oct. 23–29, 2011.
[10] T. Bressani, et al., Nuclear Instruments and Methods in Physics Research A 221 (1984) 355.
[11] M. Caria, et al., IEEE Transactions on Nuclear Science NS-32 (February (1)) (1985) 609.
[12] Mitsubishi website: ⟨http://www.mitsubishicorp.com/⟩.
[13] Hamamatsu web page: ⟨www.hamamatsu.com⟩.
[14] Maxim-Dallas web page: ⟨www.maximintegrated.com/⟩.
[15] D. Lo Presti, L. Caponetto, N. Randazzo, Nuclear Instruments and Methods in Physics Research A 602 (2009) 126, http://dx.doi.org/10.1016/j.nima.2008.12.029.
[16] National Instruments web page: ⟨www.national.com⟩.
[17] S. Riggi, et al., Nuclear Instruments and Methods in Physics Research A 624 (2010) 583.
[18] G. Drexlin, et al., Nuclear Instruments and Methods in Physics Research A 360 (1995) 245.
[19] G.A.P. Cirrone, et al., IEEE Transactions on Nuclear Science NS-51 (3) (2004) 860.
[20] EBT gafchromic film website: ⟨www.harpell.ca/manufacturer/isp/gafchromic-ebt⟩.
[21] SensL website: ⟨www.sensl.com⟩.
[22] D. Lo Presti, Patent cod. RM2012A000273 by Istituto Nazionale di Fisica Nucleare.